scientific reports

Check for updates

OPEN

Identification of pyroptosis related genes and subtypes in atherosclerosis using multiomic and single cell analysis

Kaisheng Jiang[1,8], Yang He[1,8], Bingjie Hu[2,8], Li Quan[1], Longyun Peng[3], Juntao Tian[4], Nan Zhou[5]✉, Erwen Huang[1]✉ & Qianhao Zhao[6,7]✉

Atherosclerosis (AS), the leading cause of cardiovascular diseases, is a chronic inflammatory disorder involving lipid metabolism, immune dysregulation, and cell death. Pyroptosis, a form of inflammatory programmed cell death, is implicated in AS progression, yet its molecular mechanisms and therapeutic potential remain incompletely understood. A multi-omics framework integrating transcriptomics, single-cell RNA sequencing, and machine learning to identify and prioritize pyroptosis-related genes (PRGs) in AS. Functional enrichment, immune infiltration profiling, and protein–protein interaction network analyses were conducted. Experimental validation was conducted using in vitro and in vivo models. Thirty-six PRGs were identified, with TREM2, TNF, MMP9, IL1B, and CASP1 emerging as key regulators of pyroptosis and inflammation. These PRGs demonstrated robust diagnostic potential in internal and external datasets. Immune infiltration analysis stratified AS patients into subtypes, with Cluster 2 characterized by elevated macrophage pyroptosis and a pro-inflammatory immune microenvironment. Single-cell analysis confirmed TREM2 upregulation in macrophages and monocytes, linking it to immune activation and plaque instability. Experimental validation revealed TREM2's dual role in promoting macrophage lipid accumulation and pyroptosis. This study establishes PRGs, particularly TREM2, as critical modulators of AS progression. These findings enhance our understanding of pyroptosis in AS and provide a framework for developing PRG-based diagnostic and therapeutic strategies.

Keywords Atherosclerosis, Pyroptosis, TREM2, Multi-omics analysis, Immune microenvironment

Atherosclerosis (AS) is a persistent and progressive vascular disease characterized by the thickening of arterial walls, plaque development, and lumen stenosis, making it the leading cause of cardiovascular mortality worldwide[1,2]. The severe clinical outcomes of AS, including myocardial infarction and stroke, result from the disease's disruption of normal organ function[3,4]. Despite advances in diagnostic approaches, such as lipid profiling and imaging technologies, these conventional methods often fail to detect AS at early stages or capture the dynamic and multifaceted pathological changes occurring in atherosclerotic lesions[5,6]. This highlights the urgent need for reliable molecular biomarkers that can improve early diagnosis and therapeutic strategies for AS[7,8].

[1]Faculty of Forensic Medicine, Guangdong Province Translational Forensic Medicine Engineering Technology Research Center, Zhongshan School of Medicine, Sun Yat-Sen University, Guangzhou 510080, People's Republic of China. [2]Division of Forensic Medicine, Department of Pathology, School of Basic Medical Sciences, Guangzhou Medical University, Guangzhou 511436, People's Republic of China. [3]Department of Cardiology, The First Affiliated Hospital, Sun Yat-Sen University, Guangzhou 510080, People's Republic of China. [4]Zhongshan School of Medicine, Sun Yat-Sen University, Guangzhou 510080, People's Republic of China. [5]Public Order Administration Detachment, Changsha Municipal Public Security Bureau, Changsha 410006, People's Republic of China. [6]Department of Human Anatomy, School of Basic Medical Sciences, Guangzhou University of Chinese Medicine, Guangzhou, People's Republic of China. [7]Research Centre for Basic Integrative Medicine, School of Basic Medical Sciences, Guangzhou University of Chinese Medicine, Guangzhou, People's Republic of China. [8]Kaisheng Jiang, Yang He and Bingjie Hu contributed equally to this work and shared first authorship. ✉email: 1253795947@qq.com; huangerw@mail.sysu.edu.cn; zhaoqh@gzucm.edu.cn

Pyroptosis, a regulated form of inflammatory programmed cell death, has emerged as a key factor in AS progression. Unlike apoptosis or necrosis, pyroptosis is mediated by the activation of inflammatory caspases, such as caspase-1, and is characterized by rapid plasma membrane rupture and the release of pro-inflammatory cytokines, including IL-1β and IL-18[9,10]. This process exacerbates local inflammation, recruits immune cells, and destabilizes plaques, thereby increasing the risk of cardiovascular events[11–13]. Recent studies suggest that targeting pyroptosis-related pathways may not only mitigate disease progression but also stabilize plaques, providing a promising avenue for refining both diagnostic and therapeutic strategies for AS[12–14].

To address these challenges, it is essential to understand the molecular mechanisms of pyroptosis in AS and identify key pyroptosis-related genes (PRGs) that drive the disease. Advances in high-throughput technologies, such as transcriptomics, single-cell RNA sequencing (scRNA-seq), and artificial intelligence, now enable the integrative analysis of complex datasets, offering a more comprehensive understanding of disease processes[15,16]. Machine learning algorithms, in particular, can prioritize candidate biomarkers by leveraging their predictive importance across multiple datasets[15,16]. These approaches hold great promise in unraveling the intricate interactions between PRGs and AS progression, paving the way for the discovery of novel molecular subtypes and therapeutic targets.

In this study, we employed a multi-omics framework to systematically investigate the role of PRGs in AS. By integrating bulk transcriptomic data, scRNA-seq, and machine learning techniques, we aimed to explore the diagnostic and therapeutic potential of PRGs. Our analysis identifies novel molecular subtypes of AS defined by distinct PRG expression patterns and immune infiltration profiles, providing new insights into the inflammatory microenvironment of atherosclerotic plaques. These findings lay the foundation for incorporating pyroptosis biomarkers into clinical practice, ultimately advancing personalized approaches for AS diagnosis and treatment.

Results

Identification of PRGs in AS

Using the GSE100927 dataset, which includes samples from 69 atherosclerotic arteries and 35 healthy arteries, we identified 554 Differential expressed genes (DEGs), comprising 408 upregulated genes and 146 downregulated genes (Fig. 1A-B). To identify PRGs associated with AS, we integrated these DEGs with a predefined set of PRGs, resulting in 36 overlapping genes (Fig. 1C). Functional enrichment analysis revealed that these PRGs were significantly associated with several biological processes, including the regulation of inflammatory response and IL-1β production (Fig. 1D). In the cellular components, PRGs were primarily enriched in inflammasome complex and tertiary granule (Fig. 1E). In terms of molecular functions, key terms included lipopolysaccharide binding, cytokine activity and protease binding (Fig. 1F). Kyoto Encyclopedia of Genes and Genomes (KEGG) pathway analysis highlighted the involvement of these PRGs in several inflammation-related pathways, including the NOD-like receptor signaling pathway, lipid metabolism, and Toll-like receptor signaling (Fig. 1G). These findings underscore the pivotal role of PRGs in modulating inflammatory and immune responses in AS.

Screening of key PRGs in AS

To identify key regulators of pyroptosis and inflammation in AS, we used network-based and machine learning approaches. A protein-protein interaction (PPI) network was conducted for the 36 PRGs, revealing a dense network of 30 genes by STRING and Cytoscape (Fig. 2A). Using the cytoHubba plugin, we calculated node centrality with four distinct algorithms (Degree, MNC, BottleNeck, and Stress) (Supplementary Fig. 1). The overlap of the top 10 genes identified by each algorithm yielded 9 hub genes: TNF, IL1B, TLR2, MMP9, CASP1, APOE, CCL5, TREM2 and CYBB (Fig. 2B). These genes represent critical of pyroptosis and inflammation in AS.

To further refine the selection of key genes, the predictive importance of PRGs was evaluated using 96 machine learning models, which demonstrated good predictive ability (Supplementary Fig. 2). Additionally, in 23 of these models, the average ranking of genes across models identified the most significant predictors (Fig. 2C, Supplementary Fig. 3). Additionally, LASSO (Least Absolute Shrinkage and Selection Operator) regression analysis was applied to the 9 hub genes, resulting in the retention of 8 genes (APOE, MMP9, TLR2, CASP1, IL1B, CCL5, TREM2 and TNF, Fig. 2D). Finally, the intersection of the LASSO-selected genes with the top 5 genes from machine learning rankings yield 5 core genes: TREM2, TNF, MMP9, IL1B and CASP1 (Fig. 2E). These genes likely serve as key regulators of pyroptosis and inflammation, making them potential diagnostic and therapeutic targets for AS.

Diagnostic evaluation of key PRGs in AS

To further validate the diagnostic potential of the five core genes (TREM2, TNF, MMP9, IL1B, and CASP1), we conducted internal and external validation using the GSE100927 and GSE120521 datasets. We first performed an internal validation using the GSE100927 dataset to evaluate the diagnostic performance of the five key genes. Receiver operating characteristic (ROC) curve analysis showed that all five genes achieved high Area Under the Curve (AUC) values, indicating their robust diagnostic capability for distinguishing AS samples from normal controls (Fig. 3A). In the external dataset (GSE120521), violin plots revealed significant expression differences of TREM2, MMP9, and CASP1 between stable and unstable regions of human atherosclerotic plaques (Fig. 3B). ROC curve analysis in this external dataset confirmed that these genes also exhibited high AUC values, supporting their potential as diagnostic biomarkers (Fig. 3C). These findings highlight the potential of these genes not only in distinguishing AS from normal samples but also in differentiating stable from unstable plaque regions.

Immune infiltration analysis identifies distinct immune profiles in AS subtypes

To investigate the immune landscape in AS, we performed immune infiltration analysis using CIBERSORT and IPS, comparing AS patients with healthy controls in the GSE100927 dataset. Significant differences in immune

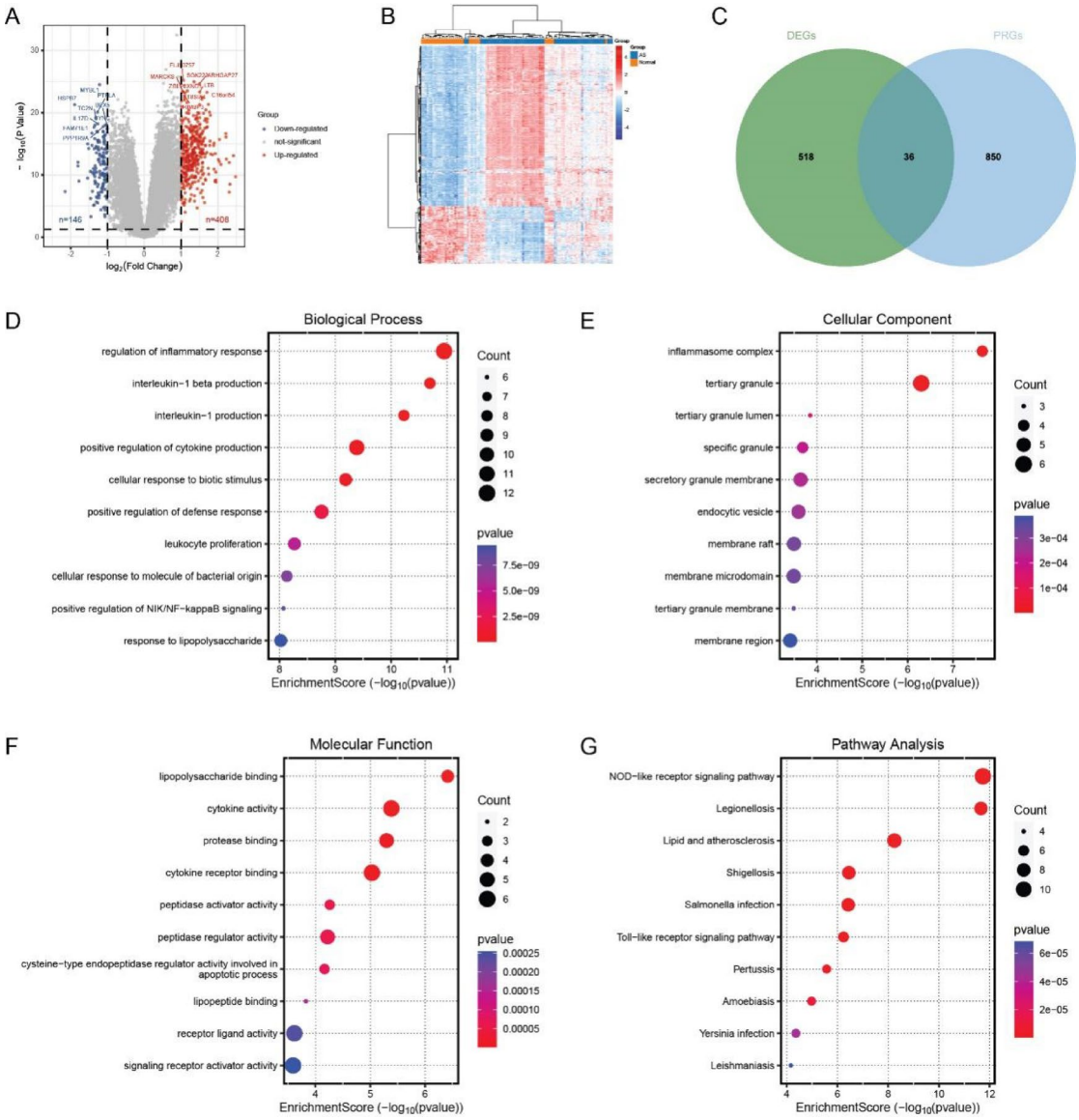

Fig. 1. Identification of PRGs in AS. (**A**) Volcano plot showing the distribution of DEGs in GSE100927, with a threshold of adjusted p-value < 0.05 and |log2 fold change| > 1. Red and blue dots represent upregulated and downregulated genes, respectively. (**B**) Heatmap of hierarchical clustering for DEGs in AS and control samples from GSE100927, with red and blue indicating higher and lower expression levels, respectively. (**C**) Venn diagram illustrating the intersection of DEGs identified in GSE100927 and a predefined PRG set, resulting in 36 overlapping genes. (**D**–**F**) GO enrichment analysis of the 36 PRGs in AS, highlighting key biological processes, cellular components, and molecular functions. **(G)** KEGG pathway analysis of PRGs in AS.

cell distributions were observed, with AS patients exhibiting higher IPS and Major Histocompatibility Complex (MHC) scores, suggesting enhanced immune response and antigen presentation (Fig. 4A-B). The co-inhibition of the Immune Checkpoint (CP) score was lower in AS patients, indicating a possible reduction in immune tolerance (Fig. 4B).

We then performed unsupervised hierarchical clustering based on their expression of the five key PRGs, dividing AS samples into two clusters, Cluster 1 and Cluster 2 (Supplementary Fig. 4A-B). Principal component analysis (PCA) confirmed distinct separation between the two clusters (Fig. 4C). All five key PRGs were significantly upregulated in Cluster 2 compared to Cluster 1 ($P < 0.001$) (Fig. 4D). Immune cell infiltration analysis showed increased levels of $CD8^+$ T cells, Tfh cells, γδ T cells, M0 macrophages, and activated mast cells in Cluster 2 (Fig. 4E, Supplementary Fig. 4C). The correlation between these PRGs and M0 macrophages further emphasizes the critical role of macrophages in regulating the immune microenvironment in AS (Fig. 4F).

Single-cell transcriptomic analysis reveals cell-type-specific expression patterns of PRGs

To further investigate the expression of five key genes in different immune cell types in AS, we analyzed the scRNA-seq dataset (GSE159677). Distinct cell populations, including T cells, B cells, NKT cells, endothelial

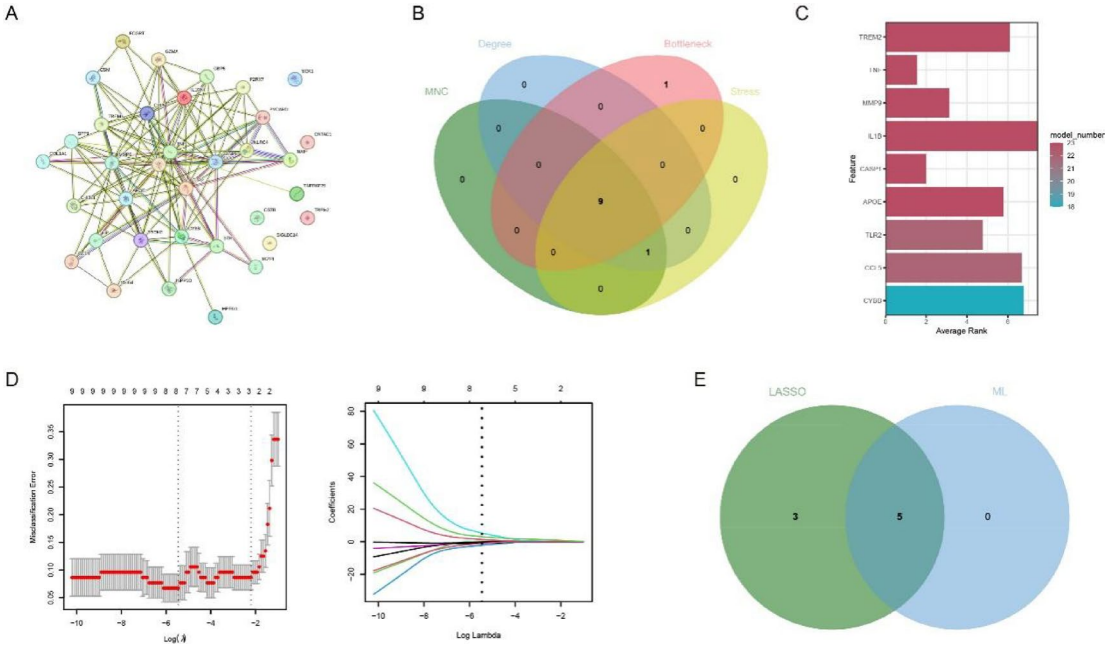

Fig. 2. Screening of key PRGs in AS. (**A**) PPI network of differentially expressed PRGs. (**B**) Venn diagram indicating the overlap of key genes identified by 4 distinct algorithms (MNC, Degree, BottleNeck and Stress) in the PPI network. (**C**) Average ranking of genes based on their performance across 23 machine learning models. (**D**) LASSO regression analysis for 9 hub genes. The left panel displays the minimum criteria for model selection, while the right panel shows the coefficient profiles of the retained genes. A total of 8 genes were retained based on the optimal lambda value. (**E**) Venn diagram indicating the overlap of 8 genes identified by LASSO regression and the top 5 ranked genes from machine learning models, resulting in 5 core genes.

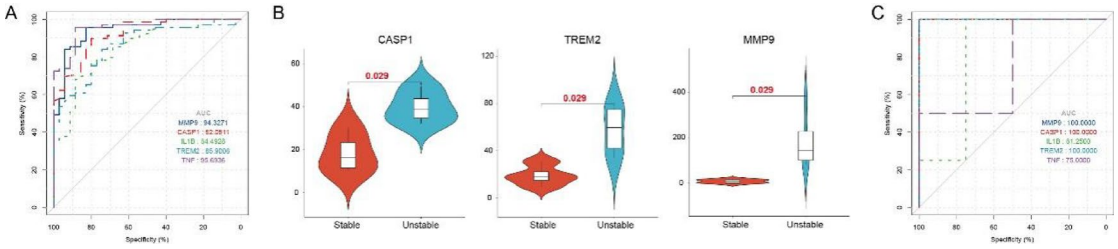

Fig. 3. Diagnostic evaluation of key PRGs in AS. (**A**) ROC curve analysis showing the diagnostic performance of key PRGs in distinguishing AS from normal samples in the GSE100927 dataset. (**B**) Violin plots depicting the expression levels of the key genes in the GSE120521 dataset, comparing stable and unstable regions. (**C**) ROC curve analysis of the diagnostic performance of key PRGs in the GSE120521 dataset.

cells, macrophages, monocytes, vascular smooth muscle cells (VSMC) and mast cells, were identified (Fig. 5A). In the atherosclerotic core (AC), macrophages and monocytes showed increased proportions, compared to patient-matched normal arterial tissue (PA), while endothelial cells and VSMCs were reduced (Fig. 5B). GO and Kyoto KEGG pathway analysis of DEGs confirmed enrichment in immune response and inflammation-related processes (Fig. 5C–D). Further, we compared the overall expression levels of the five key genes between AC and PA samples. We found that TREM2, MMP9, IL1B, and CASP1 were significantly upregulated in AC samples, while, TNF was higher in PA samples (Fig. 5E, Supplementary Fig. 5). Specifically, TREM2 expression was markedly higher in macrophages and monocytes from AC samples, further supporting its central role in immune activation in AS plaques (Fig. 5F–G).

In vivo and in vitro validation of TREM2 in atherosclerosis

Given the compelling evidence from previous analyses, we conducted experimental validation to assess the role of TREM2 in AS. In *Apoe*$^{-/-}$ mice fed a high-fat diet for 16 weeks, Trem2 mRNA and protein expression were significantly elevated in the aorta compared to WT controls ($P < 0.05$) (Fig. 6A–C). In vitro, ox-LDL treatment significantly upregulated TREM2 mRNA expression in THP-1 cells ($P < 0.01$) (Fig. 6D). To further investigate the role of TREM2, siRNA-mediated knockdown of TREM2 (siTREM2) was performed in ox-LDL-treated THP-1 cells. Western blot analysis confirmed the effective knockdown of TREM2 protein expression (Fig. 6E–

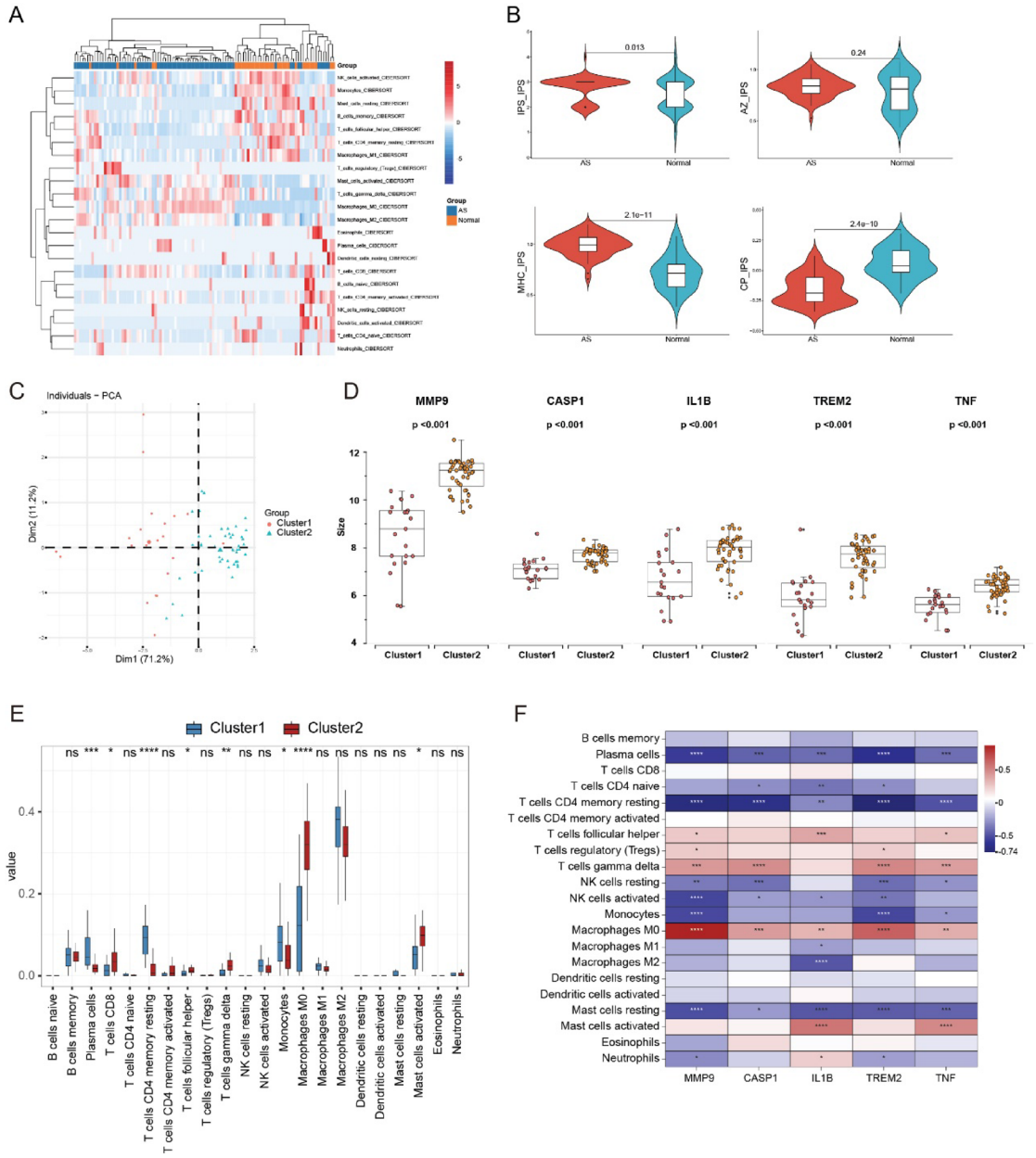

Fig. 4. Immune infiltration and cluster analysis in AS patients. (**A**) Heatmap illustrating the differences in immune cell infiltration profiles between AS patients and healthy controls based on CIBERSORT analysis. Red represents higher relative infiltration levels, while blue represents lower relative infiltration levels. (**B**) Violin plots showing the IPS of selected immune cells, demonstrating significant differences between the AS and control groups. (**C**) PCA plot illustrating the separation between Cluster1 and Cluster2 based on gene expression profiles. (**D**) Expression of five key PRGs between Cluster1 and Cluster2 ($P < 0.001$). (**E**) Box plots depicting significant differences in the relative abundance of various immune cell types between the two subtypes. The y-axis represents the relative cell proportion, and each box plot displays the median and interquartile range for each cell type. (**F**) Heatmap showing the correlation between five key PRGs and immune cell infiltration levels. The color scale represents the correlation coefficient, with red indicating a positive correlation and blue indicating a negative correlation.

F). Oil Red O staining revealed a significant reduction in lipid droplet accumulation in the siTREM2 group compared to control siRNA-transfected cells (si-NC) ($P < 0.01$) (Fig. 6G–H), indicating that TREM2 knockdown attenuated foam cell formation.

To explore the mechanism underlying TREM2-mediated pyroptosis, we examined NLRP3 inflammasome pathway activation. Western blot analysis showed that knockdown of TREM2 markedly suppressed the expression of GSDMD-N, Caspase-1 p20, NLRP3 and IL-1β ($P < 0.05$, Fig. 6I–K), indicating attenuated inflammasome activation and pyroptotic signaling. This was further supported by ELISA measurements, where the secretion

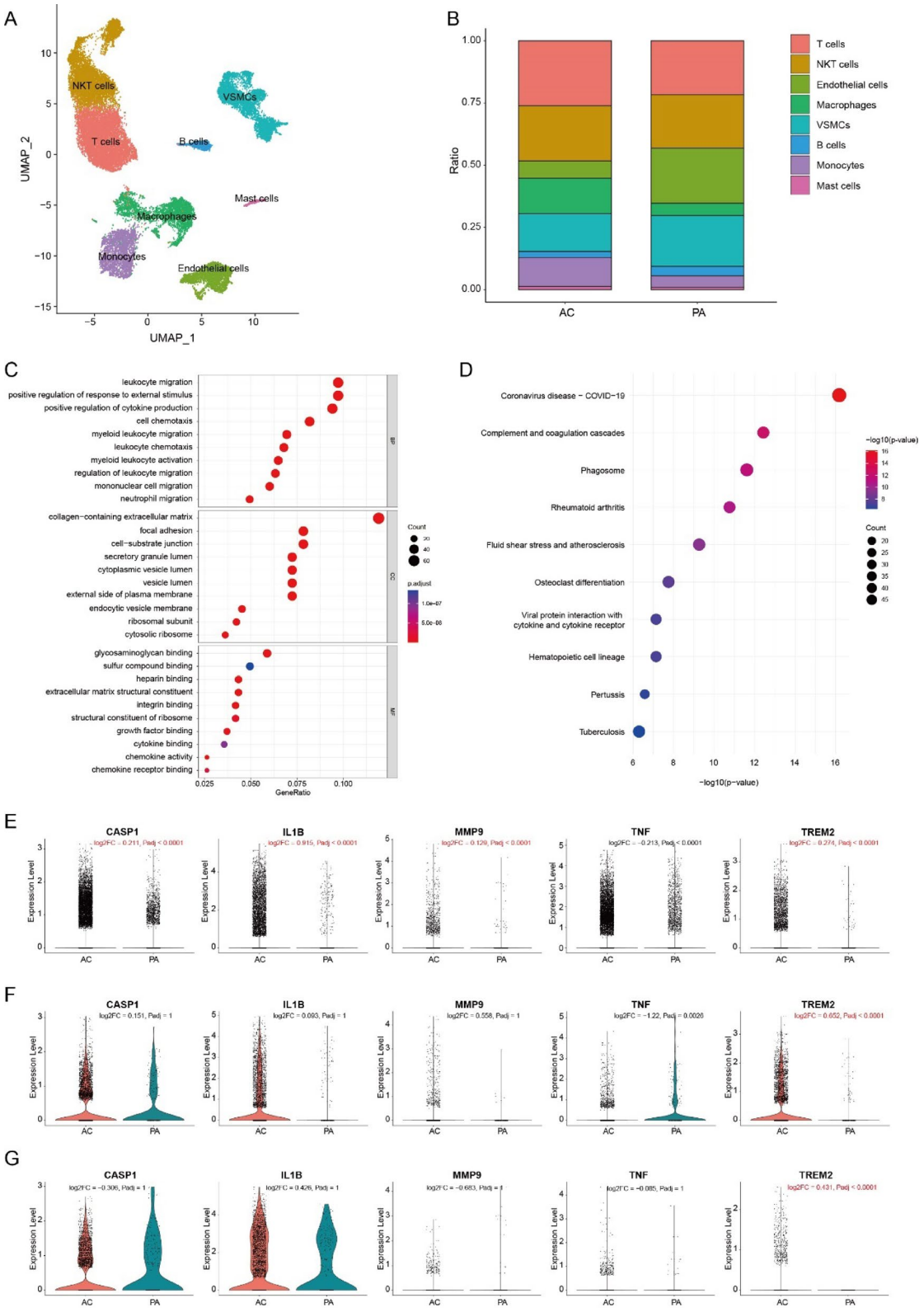

Fig. 5. Single-cell transcriptomic analysis of PRGs expression across different cell types in AS. (**A**) UMAP plot illustrating the distribution of different cell types in AC and PA samples. (**B**) Comparison of the relative proportions of different immune cell types between AC and PA samples. (**C**–**D**) GO and KEGG pathway enrichment analysis of differentially expressed genes between AC and PA samples. (**E**) Expression levels of the five key PRGs in AC and PA samples. (**F**) Expression levels of the five key PRGs in macrophages. (**G**) Expression levels of the five key PRGs in monocytes.

of IL-1β and IL-18 in the culture supernatant was significantly reduced in the si-TREM2 group ($P < 0.0001$, Fig. 6L).

Consistently, LDH release, an indicator of membrane rupture during pyroptosis, was significantly reduced in si-TREM2-transfected cells ($P < 0.001$), suggesting improved membrane integrity (Fig. 6M). Moreover, CCK-8 assays showed that knockdown of TREM2 significantly restored cell viability in ox-LDL-treated macrophages, indicating that TREM2 promotes ox-LDL-induced cytotoxicity ($P < 0.0001$, Fig. 6N).

Finally, immunofluorescence staining of aortic sections confirmed the co-localization of Trem2 with $CD68^+$ macrophages in the atherosclerotic plaques in *Apoe*$^{-/-}$ mice, supporting its functional role in plaque-resident macrophages (Fig. 6O). Collectively, these findings demonstrate that TREM2 promotes lipid accumulation, activates the NLRP3 inflammasome pathway, and induces pyroptosis in macrophages, thereby contributing to the development of atherosclerosis. These results highlight TREM2 as a potential diagnostic and therapeutic target in AS.

Discussion

AS is a chronic inflammatory disease characterized by lipid accumulation in the intima leading to complications such as myocardial infarction and stroke[17]. In the past decades, putative therapeutic strategies targeting chronic inflammation in AS have been proposed, offering potential avenues for preventing or treating the disease[18]. Pyroptosis, a form of regulated cell death that is inherently inflammatory, involves rapid plasma-membrane rupture and proinflammatory cytokines release[19]. Recent studies indicate that pyroptosis affects the entire progression of atherosclerosis[11,20,21]. Thus, targeting the molecules involved in pyroptosis could offer promising strategies for AS diagnosis and treatment.

In this study, we systematically explored the role of PRGs in AS progression through a multi-omic framework that included transcriptomic analysis, scRNA-seq, and experimental validation. Our analysis identified 36 PRGs associated with AS, which were significantly enriched in pathways regulating inflammation and immune responses, such as the NOD-like receptor and Toll-like receptor signaling pathways. These pathways have long been implicated in AS progression due to their ability to amplify local inflammation and destabilize plaques, leading to adverse cardiovascular outcomes[22–27].

Using rigorous network-based approaches and machine learning algorithms, we further prioritized five key PRGs—TREM2, TNF, MMP9, IL1B, and CASP1—as pivotal regulators of pyroptosis and inflammation. We demonstrated the robust diagnostic potential of these five PRGs, as evidenced by their high diagnostic performance in both internal and external datasets. These findings provide a foundation for developing PRG-based diagnostic tools to predict AS progression and plaque instability. Macrophage-derived foam cells are the major cells involved in AS lesions and a key factor in plaque instability[28]. The death of macrophages in advanced lesions leads to the release of growth factors, cytokines, proteases and intracellular lipids, which fuel the inflammatory response and promote necrotic core formation, increasing plaque vulnerability and the risk of thrombosis[20,29,30]. As a form of regulated necrosis that secretes pro-inflammatory factors, pyroptosis accounts for a significant portion of macrophage death in AS plaques[31]. Our immune infiltration analysis further supports the critical role of macrophage pyroptosis in AS progression.

Atherosclerotic lesions exhibit significant cellular heterogeneity and complexity. High-resolution technologies, including scRNA-seq, allow for detailed analysis of the immune cells and molecular alterations. In our study, we observed significant changes in the cellular landscape between AC and PA regions, with increased macrophage and monocyte infiltration in AC areas. In contrast, the observed reduction in endothelial cells and VSMCs in AC regions reflects a breakdown in vascular integrity and homeostasis, further exacerbating plaque vulnerability. At the molecular level, elevated expression of TREM2, MMP9, IL1B, and CASP1 in AC samples emphasizes their role in immune activation and pyroptosis regulation. Notably, the significant upregulation of TREM2 in macrophages and monocytes highlights its contribution to inflammation and plaque progression[32].

Earlier studies have suggested that TREM2 acts as a molecular switch in AS progression, regulating macrophage-mediated inflammation, lipid metabolism, and pyroptosis. TREM2 enhances lipid uptake and foam cell formation by upregulating CD36 and activating downstream pathways such as PPARγ, contributing to early plaque development[33]. Moreover, TREM2 supports macrophage survival by activating AKT/mTOR signaling pathway, preventing excessive apoptosis and promoting efferocytosis, which is critical for plaque stability in later stages[34,35]. This dual role of TREM2 is consistent with its function in neurodegenerative diseases, such as Alzheimer's disease, where it regulates lipid metabolism, microglial activation, and inflammation[36]. However, the analysis of one of the datasets used in this study suggests significant TREM2 upregulation in unstable plaques. At first glance, this upregulation may appear to contradict the previously reported role of TREM2 in macrophage survival, efferocytosis, and plaque stabilization. Nevertheless, we believe this apparent discrepancy reflects the context-dependent, stage-specific, and microenvironment-sensitive nature of TREM2's function in atherosclerosis. We hypothesize that the elevated expression of TREM2 in unstable plaques may not indicate a purely protective role but rather reflect a heightened immune response and macrophage burden, both of which are common features of vulnerable plaque microenvironments. In this context, TREM2 may function as an adaptive, or even maladaptive, responder to persistent oxidative and inflammatory stimuli in unstable plaques. Moreover, considering the differences between mechanistic gene perturbation studies (e.g., overexpression or knockdown) and observational transcriptomic data from human lesions, the elevated TREM2 expression in unstable plaques may not be purely protective. Instead, it may reflect a more complex adaptive response to the dynamic microenvironment in atherosclerotic lesions.

Our experimental validation further underscores the involvement of TREM2 in lipid metabolism and inflammatory activation, demonstrating its role in promoting macrophage lipid storage, which drives early plaque development. These findings integrate well with previous transcriptomic analyses, confirming TREM2 as a central regulator of both immune activation and pyroptosis in AS pathophysiology. In conclusion, the role

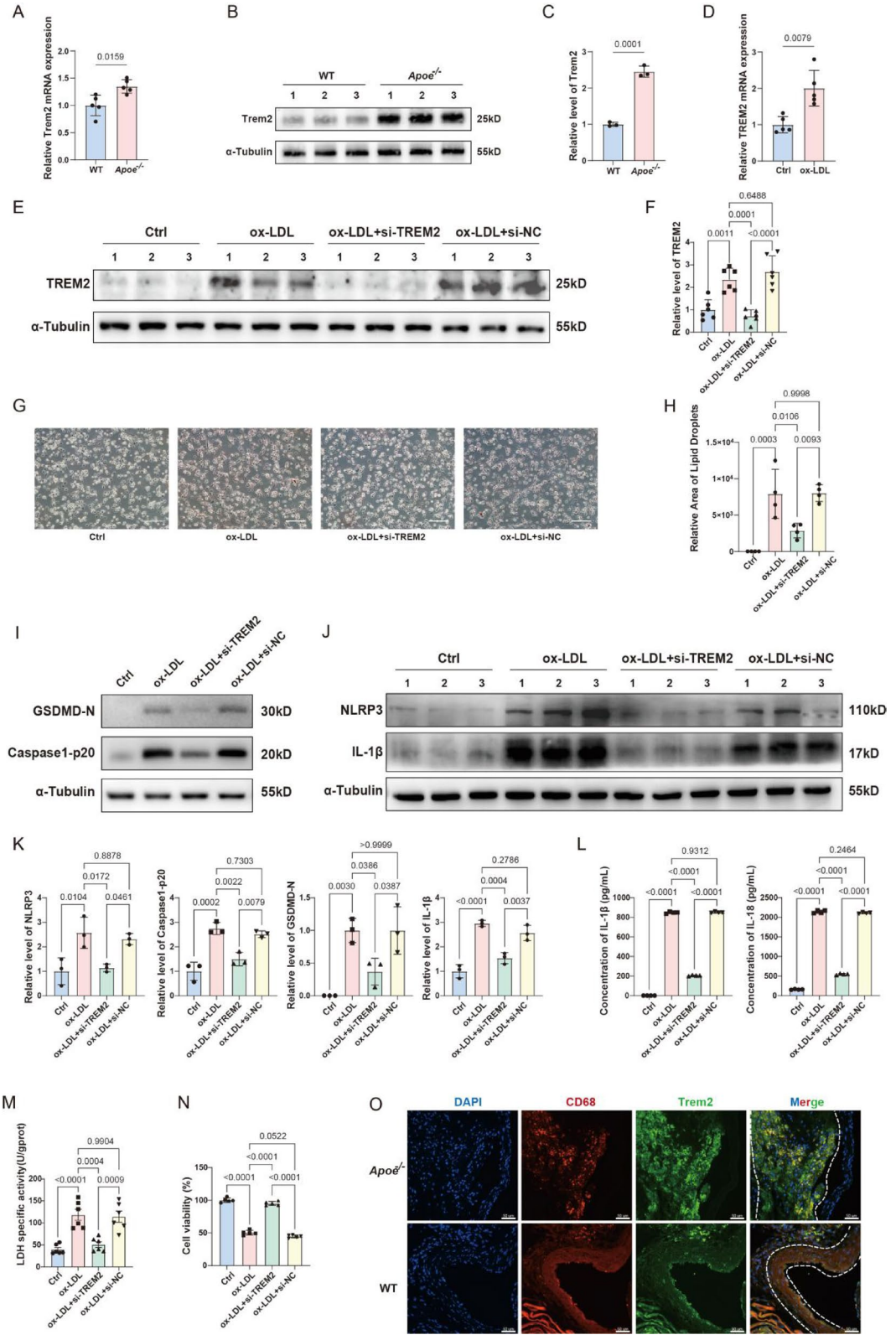

of TREM2 in atherosclerosis is multifaceted and context-dependent, with its effects varying across different stages of plaque development. Future studies integrating experimental models with clinical data are essential to fully understand the dynamic functions of TREM2 in the progression of atherosclerosis and its potential as a therapeutic target.

Building on these findings, inhibition of pyroptosis and inflammation presents a promising therapeutic strategy for atherosclerosis, complementing conventional treatments. Recent clinical trials, such as CANTOS (Canakinumab Antiinflammatory Thrombosis Outcomes Study) and LoDoCo (Low-Dose Colchicine for Secondary Prevention of Cardiovascular Disease), have validated the efficacy of anti-inflammation therapy in

◀**Fig. 6**. High expression of PRGs is associated with the development of AS. (**A**) Relative mRNA expression level of Trem2 in aortas of WT and high-fat diet-fed *Apoe*$^{-/-}$ mice ($n = 5$). (**B**–**C**) Relative protein expression levels of Trem2 in aortas of WT and high-fat diet-fed *Apoe*$^{-/-}$ mice ($n = 3$). (**D**) Relative mRNA expression levels of TREM2 in THP-1 cells and ox-LDL induced THP-1 cells ($n = 5$). (**E**–**F**) TREM2 protein expression levels in THP-1 cells, ox-LDL-induced THP-1 cells, and ox-LDL-induced THP-1 cells with or without TREM2 knockdown ($n = 6$). (**G**–**H**) Oil Red O staining of lipid accumulation in ox-LDL-stimulated THP-1 cells with or without TREM2 knockdown ($n = 4$, Scale bar = 100 μm). (**I**–**K**) Western blot analysis showing protein expression of cleaved Caspase-1 p20, GSDMD-N, NLRP3 and IL-1β in THP-1 cells under different treatments ($n = 3$). (**L**) ELISA quantification of IL-1β and IL-18 levels in the culture supernatants of ox-LDL-treated THP-1 cells ($n = 4$). (**M**) LDH specific activity levels in macrophages were measured using a commercial assay kit ($n = 6$), indicating cell membrane damage and pyroptosis activity. (**N**) Cell viability assessed by CCK-8 assay in THP-1 cells with or without TREM2 knockdown under ox-LDL stimulation ($n = 5$). (**O**) Immunofluorescence images of aortic root sections WT and high-fat diet-fed *Apoe*$^{-/-}$ mice showing Trem2 (green) expression, CD68 (red) as a macrophage marker, and DAPI (blue) for nuclear staining, Scale bar = 50 μm. Data are presented as mean ± SD.

AS. Moreover, emerging evidence suggests that pyroptosis plays a pivotal role in the molecular mechanisms underlying these therapeutic effects of these treatment[37–42]. Given the complicated pathways involved in pyroptosis, various molecular targets have been proposed for therapeutic intervention in AS. These include strategies such as regulating inflammasome components expression[43,44], inhibiting inflammasome activation[45,46], preventing inflammasome assembly[47,48], suppressing caspase-1 or GSDMD activation[49,50], and inactivating pyroptosis-related inflammatory cytokines[42,51]. Several candidate drugs targeting these pathways are currently under investigation for their efficacy in treating AS. Furthermore, the diagnostic potential of TREM2 and other key PRGs could be utilized for early detection and risk assessment in AS patients.

Despite these promising findings, several limitations need to be considered. A primary limitation is the small sample size in the validation datasets, particularly GSE120521 and GSE159677, which consist of only four and three patients, respectively. This small cohort size limits the statistical power of the analyses and the generalizability of our findings. Larger, more diverse datasets are necessary to confirm and expand on the pyroptosis-related gene signatures identified here. Additionally, the reliance on publicly available datasets may introduce selection bias, potentially limiting the generalizability of our results. Furthermore, the anatomical and clinical heterogeneity within the datasets poses additional challenges. Future studies focusing on specific arterial regions may provide more precise insights. More detailed clinical data in future studies will be essential to further investigate the role of pyroptosis in different patient subgroups. Additionally, while TREM2 was experimentally validated, the functional roles of other key PRGs remain to be fully elucidated. Future studies should focus on in-depth mechanistic investigations using in vitro and in vivo models. Furthermore, the clinical relevance of these findings needs validation in larger, independent patient cohorts to assess their utility in personalized therapy.

Conclusion

This study underscores the critical role of PRGs, particularly TREM2, in the pathogenesis of AS. By combining multi-omic and single-cell analyses with experimental validation, we provide a comprehensive framework for understanding the molecular and cellular mechanisms underlying AS. These findings not only advance our knowledge of AS pathophysiology but also offer a foundation for the developing PRG-based diagnostic and therapeutic strategies for more effective AS management.

Methods

Data sources and preprocessing

The raw gene expression data, clinical information, and single-cell RNA-seq datasets used in this study were obtained from publicly accessible databases. Microarray data and corresponding clinical information related to AS were retrieved from Gene Expression Omnibus (GEO) database under the accession number GSE100927. This dataset consists of microarray data from atherosclerotic and non-atherosclerotic tissues derived from carotid, femoral, and infra-popliteal arteries. We used all available samples from this dataset to capture a comprehensive transcriptional landscape related to pyroptosis in atherosclerosis. GSE120521 contains RNA-seq data from carotid artery plaques of four patients, which were used for independent validation of candidate genes identified in the GSE100927 discovery phase. GSE159677 provides single-cell RNA-seq data from calcified plaques of both atherosclerotic and healthy carotid arteries from three asymptomatic patients, enabling analysis of cell-type-specific pyroptosis-related gene expression.

Data related to pyroptosis were curated from GeneCards (https://www.genecards.org/), and a total of 886 PRGs were identified. These genes were then cross-referenced with the AS dataset to identify relevant candidates for further analysis.

All datasets were preprocessed to remove batch effects using the "sva" R package. Gene expression profiles were normalized using the "limma" R package. For scRNA-seq data, quality control, filtering, and normalization were performed using the "Seurat" R package.

Analyzing genes linked to pyroptosis

Differential expression analysis was performed to identify key PRGs involved in AS. The "limma" R package was used to determine differentially expressed genes (DEGs), with thresholds set at |log2 fold change| > 1 and an

Gene	Forward (5′-3′)	Reverse (5′-3′)
TREM2	ATGATGCGGGTCTCTACCAGTG	GCATCCTCGAAGCTCTCAGACT
Trem2	CTACCAGTGTCAGAGTCTCCGA	CCTCGAAACTCGATGACTCCTC
GAPDH	GTCTCCTCTGACTTCAACAGCG	ACCACCCTGTTGCTGTAGCCAA
Gapdh	CATCACTGCCACCCAGAAGACTG	ATGCCAGTGAGCTTCCCGTTCAG

Table 1. Primer sequences of RT-PCR.

adjusted p-value < 0.05. Volcano plots were generated to visualize DEGs, and a Venn diagram was constructed to intersect DEGs with the curated PRGs list, thereby highlighting potential candidates for further investigation.

Functional and pathway enrichment analysis and Protein–protein interaction (PPI) network construction

To explore the biological significance of the identified DEGs, Gene Ontology (GO) and Kyoto Encyclopedia of Genes and Genomes (KEGG) pathway enrichment analyses were conducted using the "clusterProfiler" R package. Enriched pathways related to pyroptosis were prioritized, and the results were visualized using dot plots. The interactions between the identified proteins were analyzed via the STRING online tool (http://string-db.org/), with a confidence score threshold of > 0.7 to filter interactions. To evaluate the centrality and importance of each gene in the network, four algorithms (MNC, Degree, BottleNeck, Stress) were used to rank the genes based on connectivity and network properties.

Accuracy of diagnosis

Key PRGs were selected through an extensive machine learning analysis using 96 models in R to assess their diagnostic accuracy in AS. The optimal machine learning model was used to construct a diagnostic framework and identify the most significant diagnostic genes.

Immune profiling

Immune cell infiltration was estimated utilizing the "CIBERSORT" and "Immune Phenotype Scoring (IPS)" algorithms based on gene expression profiles. The association in between PRGs expression and immune cell infiltration levels was evaluated to comprehend the immune landscape in AS.

Subtype classification

Agreement clustering was performed using the "ConsensusClusterPlus" package to categorize patients into unique molecular subtypes. The optimal number of clusters was determined based on cumulative distribution function (CDF) plots and agreement matrices. Differences in immune infiltration were also compared amongst the subtypes to identify subtype-specific immune features.

Single-cell transcriptomic analysis and copy number variation profiling

Single-cell RNA-seq data were analyzed utilizing the "Seurat" R plan to explore cellular heterogeneity in AS. Cell clusters were annotated based upon canonical markers, and t-distributed stochastic neighbor embedding (tSNE) and Uniform Manifold Approximation and Projection (UMAP) methods were used for dimensionality reduction and visualization of cell clusters. The expression patterns of PRGs across different cell types were analyzed to reveal their cell-type-specific roles.

Animals

Apoe$^{-/-}$ mice (6–8 weeks old, 18–22 g) were purchased from GemPharmatech Co., Ltd., (Jiangsu, China). The mice were housed in specific pathogen-free (SPF) conditions with a 12-hour light/dark cycle at a controlled temperature of 25 ± 1 ℃ and had ad libitum access to food and water. To establish the AS model, *Apoe*$^{-/-}$ mice were fed a high-fat diet (HFD; Junke Biological Co., Ltd., Nanjing, China) for 16 weeks. Wild-type C57BL/6 mice on a normal diet served as the control group. All experimental protocols were approved by the Animal Ethics Committee of Sun Yat-sen University (Number: SYSU-IACUC-2024-B1050). All experiments and methods were performed in accordance with relevant guidelines and regulations. The manuscript adheres to the ARRIVE guidelines for reporting of animal research.

Real-Time quantitative polymerase chain reaction (RT-qPCR)

Total RNA was extracted using the Tissue RNA Purification Kit PLUS (EZB-RN001-plus, EZBioscience, China) or the EZ-press RNA Purification Kit (B0004D, EZBioscience) according to the manufacturer's instructions. Complementary DNA (cDNA) was synthesized using the Color Reverse Transcription Kit (A0010CGQ, EZBioscience). Gene expression was quantified using the Color SYBR Green qPCR Master Mix (A0012-R2, EZBioscience). Primer sequences for gene amplification are listed in Table 1, with GAPDH serving as the housekeeping gene.

Immunofluorescence staining of tissues

Vascular tissues were fixed in cold acetone for 10 min and washed three times with phosphate-buffered saline (PBS). The tissues were then incubated in 5% bovine serum albumin (BSA) and 0.3% Triton X-100 at room temperature for 1 h. After blocking, primary antibodies were applied according to the manufacturer's instructions,

and tissues were incubated overnight at 4℃. The tissues were then washed three times with PBS and incubated with fluorescently labeled secondary antibodies for 2 h at room temperature. After staining with DAPI solution for 5 min and washing three times with PBS, the aortic root tissues were imaged using a fluorescence microscope (Nikon ECLIPSE Ni-U, Japan).

Western blot analysis

Total proteins from macrophages and arterial tissues were extracted using RIPA lysis buffer (Beyotime Biotechnology, Shanghai, China) supplemented with 1 mM PMSF (Beyotime Biotechnology, Shanghai, China). Protein concentrations were determined using a BCA Protein Assay Kit (Beyotime Biotechnology, Shanghai, China). Equal amounts of protein were separated by 10% SDS-PAGE gels and transferred to PVDF membranes. The membranes were blocked with 5% skim milk for 1 h and incubated overnight at 4℃ with the following primary antibodies: Rabbit Anti-Mouse/Human Trem2 (Cusabio, China). After washing three times with TBST, the membranes were incubated with appropriate secondary antibodies (1:10,000, Abcam, UK) for 2 h at room temperature. Protein bands were visualized using an ECL reagent (Millipore, USA) and a gel imaging system (Tanon, Shanghai, China). Relative expression levels were analyzed using Image J software.

Cell culture

Human THP-1 monocytes were (Immocell, Xiamen, China, catalog number: IM-H260) cultured in RPMI-1640 medium supplemented with 10% fetal bovine serum (FBS; Gibco, USA), 100 U/mL penicillin, and 100 U/mL streptomycin. Cells were maintained at 37℃ in a humidified atmosphere with 5% CO_2. Cells between passages 5–14 were used for experiments. To differentiate THP-1 cells into macrophages, cells were seeded at a density of 5×10^5 cells/mL in six-well culture plates and stimulated with 100 ng/mL phorbol 12-myristate 13-acetate (PMA; Sigma-Aldrich, Germany) for 48 h. Macrophages were then treated with 100 μg/mL oxidized low-density lipoprotein (ox-LDL; Guangzhou Yiyuan Biotech Co., Ltd., Guangzhou, China) for 24 h to induce foam cell formation. Untreated macrophages served as controls.

SiRNA interference

siRNA targeting TREM2 (si-TREM2) was used to knock down TREM2 expression. Scramble siRNA (si-NC) and si-TREM2 were synthesized by Tianyi Huiyuan (Beijing, China). Macrophages were transfected with 50 nM of si-NC or si-TREM2 using Lipofectamine 8000 (Beyotime Biotechnology, Shanghai, China) for 24 hours. The sequence of TREM2 siRNA was 5'-GGAAGAUGAUGGGAGGAAA-3'.

Foam cell formation by oil red O (ORO) staining

Macrophages were rinsed with PBS, fixed in 10% phosphate-buffered formalin for 10 min, and washed with PBS. Fixed cells were stained with 0.5% ORO solution (Solarbio, Beijing, China) at 37 °C for 15 min in darkness, followed by destaining with 60% isopropanol for 15 s and washed three times with PBS. ORO-stained lipid-laden macrophages were observed under a light microscope (Leica DMI8, Germany).

CCK-8 assay

THP-1 were seeded in 96-well plates in culture medium. After stimulating with 100 ng/ml PMA (phorbol-12-myristate-13-acetate) (Sigma-Aldrich) for 48 h, the cells were stimulated with ox-LDL (100 μg/mL, Solarbio, Beijing, China) for 24 h. 10 μL of CCK-8 solution (Servicebio, Wuhan, China) with fresh RPMI 1640 medium was added to each well and further incubated for 2 h at 37℃ with 5% CO_2. The absorbance at 450 nm was measured using a microplate reader (BioTek).

Elisa

Concentrations of IL-1β and IL-18 in the cell culture supernatants were determined using human ELISA kits following the manufacturer's instructions (IL-1β: Elabscience E-EL-H0149; IL-18: Elabscience E-EL-H0253).

LDH release measurement

Lactate dehydrogenase (LDH) release was measured to assess cell membrane damage due to pyroptosis. Supernatants were collected, and LDH levels were quantified using an LDH assay kit (E-BC-K046-M, Elabscience) according to the manufacturer's protocol. Absorbance was measured at 450 nm using a microplate reader (Tecan Sunrise™, Austria).

Statistical analysis

Statistical analyses were performed using GraphPad Prism 9 software (GraphPad, CA). Data are presented as mean ± standard deviation (SD). For comparisons between two groups, the Mann-Whitney U test was used for $n \leq 5$ or abnormally distributed data, while the two-tailed unpaired Student's t-test was used for $n > 5$ data points with a normal distribution. For comparisons among multiple groups, the Kruskal-Wallis test followed by Dunn's test was applied. A p-value of < 0.05 was considered statistically significant.

Data availability

All data supporting the findings of this study are available within the paper and its Supplementary Information.

Received: 29 December 2024; Accepted: 27 May 2025
Published online: 01 July 2025

References

1. Falk, E. Pathogenesis of atherosclerosis. *J. Am. Coll. Cardiol.* **47**, C7–12. https://doi.org/10.1016/j.jacc.2005.09.068 (2006).
2. Fan, J., Watanabe, T. & Atherosclerosis Known and unknown. *Pathol. Int.* **72**, 151–160. https://doi.org/10.1111/pin.13202 (2022).
3. Libby, P. The changing landscape of atherosclerosis. *Nature* **592**, 524–533. https://doi.org/10.1038/s41586-021-03392-8 (2021).
4. Zhu, Y. et al. Research progress on the relationship between atherosclerosis and inflammation. *Biomolecules* **8** https://doi.org/10.3390/biom8030080 (2018).
5. Frostegård, J. Immunity, atherosclerosis and cardiovascular disease. *BMC Med.* **11**, 117. https://doi.org/10.1186/1741-7015-11-117 (2013).
6. Hansson, G. K. & Hermansson, A. The immune system in atherosclerosis. *Nat. Immunol.* **12**, 204–212. https://doi.org/10.1038/ni.2001 (2011).
7. Pedro-Botet, J., Climent, E. & Benaiges, D. Atherosclerosis and inflammation. New therapeutic approaches. *Med. Clin. (Barc.)* **155**, 256–262. https://doi.org/10.1016/j.medcli.2020.04.024 (2020).
8. Riccardi, G., Giosuè, A., Calabrese, I. & Vaccaro, O. Dietary recommendations for prevention of atherosclerosis. *Cardiovasc. Res.* **118**, 1188–1204. https://doi.org/10.1093/cvr/cvab173 (2022).
9. Du, T. et al. Pyroptosis, metabolism, and tumor immune microenvironment. *Clin. Transl Med.* **11**, e492. https://doi.org/10.1002/ctm2.492 (2021).
10. Loveless, R., Bloomquist, R. & Teng, Y. Pyroptosis at the forefront of anticancer immunity. *J. Exp. Clin. Cancer Res.* **40**, 264. https://doi.org/10.1186/s13046-021-02065-8 (2021).
11. Zhaolin, Z., Guohua, L., Shiyuan, W. & Zuo, W. Role of pyroptosis in cardiovascular disease. *Cell Prolif.* **52**, e12563. https://doi.org/10.1111/cpr.12563 (2019).
12. Rao, Z. et al. Pyroptosis in inflammatory diseases and cancer. *Theranostics* **12**, 4310–4329. https://doi.org/10.7150/thno.71086 (2022).
13. Vasudevan, S. O., Behl, B. & Rathinam, V. A. Pyroptosis-induced inflammation and tissue damage. *Semin. Immunol.* **69**, 101781. https://doi.org/10.1016/j.smim.2023.101781 (2023).
14. Wei, Y. et al. GSDME-mediated pyroptosis promotes the progression and associated inflammation of atherosclerosis. *Nat. Commun.* **14**, 929. https://doi.org/10.1038/s41467-023-36614-w (2023).
15. Wang, J. et al. Identification of immune cell infiltration and diagnostic biomarkers in unstable atherosclerotic plaques by integrated bioinformatics analysis and machine learning. *Front. Immunol.* **13**, 956078. https://doi.org/10.3389/fimmu.2022.956078 (2022).
16. Fu, Y. et al. Unveiling the role of ABI3 and hub senescence-related genes in macrophage senescence for atherosclerotic plaque progression. *Inflamm. Research: Official J. Eur. Histamine Res. Soc. … Et Al].* **73**, 65–82. https://doi.org/10.1007/s00011-023-01817-w (2024).
17. Xing, Y. & Lin, X. Challenges and advances in the management of inflammation in atherosclerosis. *J. Adv. Res.* https://doi.org/10.1016/j.jare.2024.06.016 (2024).
18. Bäck, M. & Hansson, G. K. Anti-inflammatory therapies for atherosclerosis. *Nat. Rev. Cardiol.* **12**, 199–211. https://doi.org/10.1038/nrcardio.2015.5 (2015).
19. Man, S. M., Karki, R. & Kanneganti, T. D. Molecular mechanisms and functions of pyroptosis, inflammatory caspases and inflammasomes in infectious diseases. *Immunol. Rev.* **277**, 61–75. https://doi.org/10.1111/imr.12534 (2017).
20. Lin, J. et al. Oxidized low density lipoprotein induced caspase-1 mediated pyroptotic cell death in macrophages: implication in lesion instability? *PloS One* **8**, e62148. https://doi.org/10.1371/journal.pone.0062148 (2013).
21. He, B. et al. Role of pyroptosis in atherosclerosis and its therapeutic implications. *J. Cell. Physiol.* **236**, 7159–7175. https://doi.org/10.1002/jcp.30366 (2021).
22. Hoseini, Z. et al. NLRP3 inflammasome: Its regulation and involvement in atherosclerosis. *J. Cell. Physiol.* **233**, 2116–2132. https://doi.org/10.1002/jcp.25930 (2018).
23. Grebe, A., Hoss, F. & Latz, E. NLRP3 inflammasome and the IL-1 pathway in atherosclerosis. *Circul. Res.* **122**, 1722–1740. https://doi.org/10.1161/circresaha.118.311362 (2018).
24. Vallejo, J. G. Role of toll-like receptors in cardiovascular diseases. *Clin. Sci. (London, England,1979)* **121**, 1–10. https://doi.org/10.1042/cs20100539 (2011).
25. Edfeldt, K., Swedenborg, J., Hansson, G. K. & Yan, Z. Q. Expression of toll-like receptors in human atherosclerotic lesions: A possible pathway for plaque activation. *Circulation* **105**, 1158–1161 (2002).
26. Geng, H. L. et al. Increased expression of toll like receptor 4 on peripheral-blood mononuclear cells in patients with coronary arteriosclerosis disease. *Clin. Exp. Immunol.* **143**, 269–273. https://doi.org/10.1111/j.1365-2249.2005.02982.x (2006).
27. Li, H. & Sun, B. Toll-like receptor 4 in atherosclerosis. *J. Cell. Mol. Med.* **11**, 88–95. https://doi.org/10.1111/j.1582-4934.2007.00011.x (2007).
28. Moore, K. J., Sheedy, F. J. & Fisher, E. A. Macrophages in atherosclerosis: A dynamic balance. *Nat. Rev. Immunol.* **13**, 709–721. https://doi.org/10.1038/nri3520 (2013).
29. Kockx, M. M. & Herman, A. G. Apoptosis in atherosclerosis: Beneficial or detrimental? *Cardiovasc. Res.* **45**, 736–746. https://doi.org/10.1016/s0008-6363(99)00235-7 (2000).
30. Seimon, T. & Tabas, I. Mechanisms and consequences of macrophage apoptosis in atherosclerosis. *J. Lipid Res.* **50 Suppl**, 382–387. https://doi.org/10.1194/jlr.R800032-JLR200 (2009).
31. Martinet, W., Coornaert, I., Puylaert, P. & De Meyer, G. R. Macrophage death as a Pharmacological target in atherosclerosis. *Front. Pharmacol.* **10**, 306. https://doi.org/10.3389/fphar.2019.00306 (2019).
32. Makuch, M., Stepanechko, M. & Bzowska, M. The dance of macrophage death: the interplay between the inevitable and the microenvironment. *Front. Immunol.* **15**, 1330461. https://doi.org/10.3389/fimmu.2024.1330461 (2024).
33. Guo, X. et al. TREM2 promotes cholesterol uptake and foam cell formation in atherosclerosis. *Cell. Mol. Life Sci.* **80**, 137. https://doi.org/10.1007/s00018-023-04786-9 (2023).
34. Patterson, M. T. et al. Trem2 promotes foamy macrophage lipid uptake and survival in atherosclerosis. *Nat. Cardiovasc. Res.* **2**, 1015–1031. https://doi.org/10.1038/s44161-023-00354-3 (2023).
35. Piollet, M. et al. TREM2 protects from atherosclerosis by limiting necrotic core formation. *Nat. Cardiovasc. Res.* **3**, 269–282. https://doi.org/10.1038/s44161-024-00429-9 (2024).
36. Li, R. Y. et al. TREM2 in the pathogenesis of AD: a lipid metabolism regulator and potential metabolic therapeutic target. *Mol. Neurodegen.* **17** https://doi.org/10.1186/s13024-022-00542-y (2022).
37. Li, T., Zheng, G., Li, B., Tang, L. & Pyroptosis A promising therapeutic target for noninfectious diseases. *Cell. Prolif.* **54**, e13137. https://doi.org/10.1111/cpr.13137 (2021).
38. Nguyen, T. T. et al. Mitochondria-associated programmed cell death as a therapeutic target for age-related disease. *Exp. Mol. Med.* **55**, 1595–1619. https://doi.org/10.1038/s12276-023-01046-5 (2023).
39. You, R. et al. Pyroptosis and its role in autoimmune disease: A potential therapeutic target. *Front. Immunol.* **13**, 841732. https://doi.org/10.3389/fimmu.2022.841732 (2022).
40. Libby, P. & Everett, B. M. Novel antiatherosclerotic therapies. *Arterioscler. Thromb. Vasc. Biol.* **39**, 538–545. https://doi.org/10.1161/atvbaha.118.310958 (2019).
41. Nidorf, S. M., Eikelboom, J. W., Budgeon, C. A. & Thompson, P. L. Low-dose Colchicine for secondary prevention of cardiovascular disease. *J. Am. Coll. Cardiol.* **61**, 404–410. https://doi.org/10.1016/j.jacc.2012.10.027 (2013).

42. Ridker, P. M. et al. Antiinflammatory therapy with Canakinumab for atherosclerotic disease. *N. Engl. J. Med.* **377**, 1119–1131. https://doi.org/10.1056/NEJMoa1707914 (2017).
43. Kong, F. et al. Atorvastatin suppresses NLRP3 inflammasome activation via TLR4/MyD88/NF-κB signaling in PMA-stimulated THP-1 monocytes. *Biomed. Pharmacother. Biomed. Pharmacother.* **82**, 167–172. https://doi.org/10.1016/j.biopha.2016.04.043 (2016).
44. Wu, L. M. et al. Atorvastatin inhibits pyroptosis through the LncRNA NEXN-AS1/NEXN pathway in human vascular endothelial cells. *Atherosclerosis* **293**, 26–34. https://doi.org/10.1016/j.atherosclerosis.2019.11.033 (2020).
45. Abderrazak, A. et al. Anti-inflammatory and antiatherogenic effects of the NLRP3 inflammasome inhibitor arglabin in ApoE2.Ki mice fed a high-fat diet. *Circulation* **131**, 1061–1070. https://doi.org/10.1161/circulationaha.114.013730 (2015).
46. Çimen, I. et al. Prevention of atherosclerosis by bioactive palmitoleate through suppression of organelle stress and inflammasome activation. *Sci. Transl. Med.* **8**, 358ra126. https://doi.org/10.1126/scitranslmed.aaf9087 (2016).
47. Martínez, G. J., Celermajer, D. S. & Patel, S. The NLRP3 inflammasome and the emerging role of Colchicine to inhibit atherosclerosis-associated inflammation. *Atherosclerosis* **269**, 262–271. https://doi.org/10.1016/j.atherosclerosis.2017.12.027 (2018).
48. Misawa, T. et al. Microtubule-driven Spatial arrangement of mitochondria promotes activation of the NLRP3 inflammasome. *Nat. Immunol.* **14**, 454–460. https://doi.org/10.1038/ni.2550 (2013).
49. Li, Y. et al. VX-765 attenuates atherosclerosis in ApoE deficient mice by modulating VSMCs pyroptosis. *Exp. Cell Res.* **389** https://doi.org/10.1016/j.yexcr.2020.111847 (2020).
50. Hu, J. J. et al. FDA-approved Disulfiram inhibits pyroptosis by blocking gasdermin D pore formation. *Nat. Immunol.* **21**, 736–745. https://doi.org/10.1038/s41590-020-0669-6 (2020).
51. Zeng, C., Wang, R. & Tan, H. Role of pyroptosis in cardiovascular diseases and its therapeutic implications. *Int. J. Biol. Sci.* **15**, 1345–1357. https://doi.org/10.7150/ijbs.33568 (2019).

Acknowledgements

This work was supported by the National Natural Science Foundation of China (Grant Nos. 81901919 and 81920108021), and the Natural Science Foundation of Guangdong Province (Grant No. 2020A1515010078), and the Guangzhou Municipal Science and Technology Project (Grant No. 202102080092).

Author contributions

K.J.: Data curation, Formal analysis, Methodology, Software, Visualization and Writing—original draft. Y.H.: Data curation, Formal analysis, Methodology, Software, Visualization and Writing—original draft. B.H.: Formal analysis, Funding acquisition, Methodology and Writing—original draft. L.Q.: Supervision and Writing—review & editing. L.P.: Supervision and Writing—review & editing. J.T.: Data curation and Supervision. N.Z.: Conceptualization, Funding acquisition, Supervision and Writing—review & editing.Erwen Huang: Conceptualization, Project administration, Resources and Writing—review & editing. Q.Z.: Conceptualization, Funding acquisition, Project administration, Supervision, Writing—original draft and Writing—review & editing.

Declarations

Competing interests

The authors declare no competing interests.

Additional information

Supplementary Information The online version contains supplementary material available at https://doi.org/10.1038/s41598-025-04398-2.

Correspondence and requests for materials should be addressed to N.Z., E.H. or Q.Z.